Title: The neuron mixer and its impact on human brain dynamics

Authors: Charlotte E. Luff[1,2]†, Robert Peach[1,2,3]†, Emma-Jane Mallas[1,4], Edward Rhodes[1,2], Felix Laumann[5], Edward S. Boyden[6,7], David J. Sharp[1,4,8], Mauricio Barahona[5], Nir Grossman[1,2]*

Affiliations:

[1]Department of Brain Sciences, Imperial College London; London, United Kingdom.

[2]UK Dementia Research Institute, Imperial College London; London, United Kingdom.

[3]Department of Neurology, University Hospital Würzburg; Würzburg, Germany.

[4]UK Dementia Research Institute, Care Research & Technology Centre; London, United Kingdom.

[5]Department of Mathematics, Imperial College London; London, United Kingdom.

[6]Department of Brain and Cognitive Sciences, Massachusetts Institute of Technology; Cambridge, USA.

[7]Howard Hughes Medical Institute; Chevy Chase, USA.

[8]Centre for Injury Studies, Imperial College London; London, United Kingdom.

*Corresponding author. Email: nirg@ic.ac.uk

†These authors contributed equally to this work.

Abstract: A signal mixer made of a transistor facilitates rich computation that has been the building block of modern telecommunication. Here we report that a neural cell is also a signal mixer. We found through *ex vivo* and *in vivo* measurements that individual neurons mix exogenous (controlled) and endogenous (spontaneous) subthreshold membrane potential oscillations, thereby producing new oscillations. Furthermore, we demonstrate that the neural mixing dynamic is evident in human brain activity and is associated with our cognitive functions. Neural network oscillations have been observed in nearly every cognitive domain and species. Signal mixing enables single neurons to actively sculpt their network oscillations and utilize them for computational operations, which have only been seen in modern telecommunication until now.

One-Sentence Summary:

We report that a neuron is a signal mixer akin to an electronic transistor capable of modulating oscillatory human brain dynamics.

Main Text: A mixer is a device capable of multiplying signals to produce new frequencies, such as the difference and sum of the original frequencies. A signal mixer made of a transistor, or a diode, has been the building block of modern telecommunication, facilitating the critical conversion to/from higher frequency bands where transmission efficiency is high (aka heterodyning), decoding phase information, and combining multiple signals into one data stream (aka multiplexing) (*1*, *2*). Here we report for the first time that a single neural cell behaves as a signal mixer and that the neural mixing is evident in the human brain and linked to our cognitive functions.

Mixing of exogenous membrane potentials in individual neurons

We first examined whether neurons could mix exogenous (controlled) subthreshold membrane oscillations. We applied extracellular sinusoidal electric currents containing two different frequencies (f_1 and f_2) with a difference frequency (Δf) within the normal range of neural activity and recorded the induced transmembrane potentials in individual neural cells *ex vivo* using whole-cell patch clamp recording (**Fig. 1A**). We focused on the subthreshold response of the cells because suprathreshold spikes at the difference frequency could also be induced by a simple linear summation rather than mixing. We found that electrical stimulation with two sinusoids at frequencies within the normal range of neural activity (i.e., f_1 = 47 Hz and f_2 = 57 Hz) induced subthreshold membrane potential oscillations at their difference frequency (Δf = 10 Hz) (**Fig. 1B**, note that the stimulation voltages mask the subthreshold oscillations at the input frequencies f_1 and f_2).

The induction of a subthreshold membrane oscillation at the difference frequency was consistent across a wide range of stimulation frequencies, spanning three orders of magnitude. **Figure 1C** and **Figure 1D** show the subthreshold membrane oscillation induced by electrical stimulation with two sinusoids at frequencies in the upper boundary of neural activity (i.e., f_1 = 497 Hz and f_2 = 507 Hz, Δf= 10 Hz) and beyond the range of neural activity (i.e., f_1 = 4.997 kHz and f_2 = 5.007 kHz, Δf= 10 Hz) as in temporal interference (TI) stimulation (*3*), respectively. **Figure 1E** summarizes the induced oscillation amplitude at Δf across this range of applied frequencies (tested against the measurement system's intermodulation distortion, IMD, at Δf (*4*), i.e., mixing products due to hardware nonlinearity measured in the same way but without brain slices). See **fig. S1-2** panels i-ii for all membrane potential traces and statistical analyses. The amplitude of the induced Δf oscillation was smaller when the stimulation was applied at kHz frequencies. Increasing the amplitude of the applied currents evoked action potential trains at Δf, with a higher current density threshold at kHz frequencies (repeated-measures ANOVA F(5,135) = 22.3, p = 5e-17, **Fig. 1F**).

The membrane potential power spectra also showed peaks in the sum ($\sum f$) and second harmonics ($2f_1$, $2f_2$) of the applied frequencies (**Fig. 1B-D**, panel ii) as predicted by signal mixing. However, the low membrane oscillation amplitudes at those high frequencies were within the range of the measurement's IMD (rendering these measurements inconclusive) except in the lowest stimulation frequencies (i.e., f_1 = 7 Hz and f_2 = 17 Hz) when the induced frequencies were within the normal range of neural activity (i.e., $\sum f$ = 24 Hz, $2f_1$ = 14 Hz, $2f_2$ = 34 Hz). See **fig. S1-2** panels iii-iv and **fig. S3A** for all membrane potential traces and statistical analyses of the sum frequency, and **fig. S3B-C** for statistical analyses of the harmonic frequencies. These results suggest that in addition to the difference frequency, neurons are capable of producing the sum frequency and harmonics of their membrane oscillations. Interestingly, we also found significant subthreshold membrane oscillations at the first harmonic

of the difference frequency (i.e., $2\Delta f$ = 20 Hz; **fig. S3D**), suggesting the neurons are capable of further mixing the mixing products.

Origin of neuronal mixing characterized via pharmacological manipulation

We next explored the cellular origin of the subthreshold signal mixing. We hypothesized that mixing could emerge from the nonlinear summation of synaptic currents (*5–8*). We hence repeated the experiment with a subset of the stimulation frequencies and a pharmacological blockade of the synaptic ligand-gated ion channels (using NBQX, α-amino-3-hydroxy-5-methyl-4-isoxazolepropionic acid (AMPA) receptor antagonist; DAP-5, N-Methyl-D-aspartic acid (NMDA) receptor antagonist; and Bicuculline, γ-Aminobutyric acid type A (GABA-A) antagonist). We found that blocking the synaptic ion channel currents suppressed the oscillation mixing at frequencies in the normal range of neural activity (i.e., f_1 = 47 Hz and f_2 = 57 Hz), **Fig. 2A**. However, interestingly, it did not affect the mixing of oscillations at kHz frequencies beyond the normal neural range (i.e., f_1 = 4.997 kHz and f_2 = 5.007 kHz), **Fig. 2B**, implying a different biophysical underpinning at this frequency range. A recent computational study suggested that kHz TI neurostimulation may be mediated by the nonlinear rectification of the voltage-gated sodium channels (*9*). We hence repeated the experiment in the kHz range with a pharmacological blockade of these channels (using tetrodotoxin, TTX). We found that blocking the TTX-sensitive sodium channels suppressed the mixing of the membrane oscillations, **Fig. 2C**, implying their involvement in mixing kHz currents as in TI neural stimulation.

Mixing of endogenous membrane potentials in individual neurons

After confirming that neurons mix exogenous signals, we next examined whether they also mix endogenous (spontaneous) subthreshold membrane potential fluctuations. If the membrane potential polarizes at frequencies f_1 and f_2 (f_2>f_1), and those frequencies are mixed by the membrane, then the instantaneous phases of the frequencies f_1, f_2 and $\Delta f = f_2$-f_1 must be dependent, i.e., the frequency triplet must show a three-way, but not a pairwise, phase dependency (*10*). Similarly, the instantaneous phases of the triplet f_1, f_2 and $\sum f = f_1$+f_2, the triplet f_1, Δf, and $\sum f$, and the triplet f_2, Δf, and $\sum f$, must also show a three-way phase dependency. We repeated the *ex vivo* experiment but now we recorded the transmembrane potentials without electrical stimulation and then assessed the joint phase interaction of all possible frequency-mixing quadruplets (i.e., roots: f_1, f_2; products: Δf, $\sum f$) for frequencies within the normal range of neural activity (i.e., up to 250 Hz) using a nonparametric test based on the Lancaster interaction measure (*11–13*) (**Fig. 3A**; see **fig. S4** for sensitivity analysis).

We found significant frequency mixing in the spontaneous fluctuations of the neural membrane potential (joint high-order interaction (JHOI) amplitude 0.55 ±0.2, mean ±standard deviation, st.d.; n=10 cells from 10 slices and 9 animals; p = 0.0027, paired t-test against surrogate data), with a myriad of frequency mixing clusters (**Fig. 3B**). The mixings produced a broad range of new frequencies peaking at the beta and low-gamma bands. The mixing clusters between the beta and gamma bands, and between the gamma bands, were consistent across the cells (**Fig. 3C**). Adding a pharmacological blockade of the synaptic ion channel currents (as before) reduced the overall frequency mixing strength in the neural membrane potentials by approximately 30% (**fig. S5A**), particularly in a subset of high-frequency mixing clusters (**fig. S5B-C**).

To explore whether endogenous membrane potential mixing also occurs in the live brain, we recorded the membrane potentials of individual neural cells *in vivo*, using automated whole-cell patch-clamp recordings (*14*) and deployed the same computation strategy to assess the phase dependency in all possible frequency-mixing quadruplets. We found significant frequency

mixing in the spontaneous membrane potentials of the cells (0.596 ± 0.168, mean ± st.d.; n = 8 cells from 8 animals; p = 0.009). The membrane potentials of individual cells exhibited a variety of frequency mixing clusters, as in brain slices. The mixings produced a narrower range of frequencies in the beta and gamma bands (**Fig. 3D**). Across the cells, the frequency mixing clusters were consistent in the gamma bands (**Fig. 3E**).

Mixing of endogenous neural network oscillations in the human brain

After establishing that neural cells mix their subthreshold membrane oscillations, we aimed to explore whether the mixing phenomenon could affect neural network oscillations – an emerging property of synchronized membrane oscillations across thousands of coupled neurons (*15–17*). Earlier studies by us (*3*) and others (*10*, *18*), showed the feasibility of this effect in rodents. We aimed to test whether such a neural oscillation mixing exists in the human brain and, if yes, whether it has functional relevance. Neural oscillations are ubiquitous in the human brain (*19*). The most salient oscillation is the so-called alpha oscillation that can be readily observed with the naked eye in posterior scalp electroencephalography (EEG) during an awake eyes-closed state (*20*). This posterior alpha oscillation has been associated with top-down modulation of our visual attention, thereby shaping our perception and cognition (*21*, *22*). We recorded awake eyes-closed EEG in healthy human subjects (n = 20, mean age 29.3 ± 12.2 st.d., 6 females) and subsequently measured their visual attention control using a feature-matching task (*23*). We used the same computation strategy to examine the phase interaction in all possible frequency mixing quadruplets (up to 45 Hz) in EEG electrodes at a subset of sites in the parieto-occipital, temporal, and prefrontal regions (i.e., Pz, Oz, T7, T8, FP1, FP2 of the international 10-10 system) implicated in visual attention control (**Fig. 4A**).

We found a robust mixing of neural network oscillations between sites of the human brain (JHOI amplitude 0.4 ± 0.008, mean ± st.d., p = 1.6e-16, paired t-test vs surrogate data). The spatial topology of the mixing is shown in **Figure 4B**, and the frequency band topology is shown in **Figure 4C**. The inter-site mixings occurred between all brain regions and frequency bands (**fig. S6A-C**) yet was stronger between the delta and theta bands. We additionally found mixing within brain sites, i.e., between local oscillations (JHOI amplitude 0.4 ± 0.02, mean ± st.d., p = 7.2e-12). The local mixings also occurred in all brain regions and frequency bands (**fig. S6D-F**), yet each brain region displayed a unique frequency band mixing pattern (**Fig. 4D-F**). The frontal region was dominated by theta-alpha mixing; parieto-occipital, by alpha mixing; and temporal regions, by beta mixing. The strength of oscillation mixing was not correlated with the oscillation power (**fig. S7A**), implying that mixing is a distinct property of the brain oscillation dynamics.

As expected, the participants awake-eyes-closed EEG was dominated by a strong alpha oscillation (**fig S7B**). We found that the mixing strength of this alpha oscillation was correlated with the participants' visual attention capacity, indexed by the score in the subsequential feature-matching task (**Fig. 5A**, R^2= 0.363, p=0.017, linear regression). A further investigation revealed that the alpha oscillation mixings associated with visual attention were specific to those with the beta oscillation (**Fig. 5B**, R^2= 0.497, p=0.003, linear regression with Bonferroni correction for multiple comparisons). These alpha-beta mixings were strongest within the occipital cortex and between the occipital (alpha oscillation) and parietal (beta oscillation) cortices (**Fig. 5C**, repeated-measures ANOVA F(2.48), p=1.06e-5), producing new oscillations that were strongest in the gamma band (posteriorly) and weakest in the delta band (**Fig. 5D,** repeated-measures ANOVA Oz-Oz F(2.6), p=1.18e-5; Oz-Pz F(2.98), p=8.5e-7). These results suggest that our

visual attention capacity may be modulated by the efficiency by which the salient posterior alpha oscillation is mixed to augment local synchronization in the gamma band.

Concluding remarks

We report the discovery that a neural cell is a signal mixer akin to an electronic transistor or a diode. An earlier computational study theorized that a mixing phenomenon could emerge from the neurons' threshold firing property (*24*); however, there has not been any experimental evidence of a single cell mixing to date. We (*3*) and others (*10*, *18*) have observed mixing-like interactions in the oscillations of neural networks in the rodent's brain. However, since linear network interactions could explain some of these observations, no direct evidence of neural mixing was made. An example of such a linear interaction at the network level is when two neural populations oscillating at different frequencies synapse with a third population to induce firing at the difference frequency due to the periodic increase in the summed input rate. Our findings demonstrate a single-cell subthreshold mixing and suggest that the cell's mixing capability originates in the nonlinearity of the subthreshold currents via the synaptic ligand-gated ion channels or the voltage-gated sodium channels, depending on the frequency range.

We expand on the single-cell mixing discovery and show mixing of neural network oscillations in the human brain. Neural network oscillations are ubiquitous in the human brain (*19*) and implicated in regulating behavioral states (*25*), coordination of multisensory processing (*26*), and cognitive processes, such as memory and consciousness (*27*). Aberrant oscillations have been associated with almost all neurological and psychiatric disorders (*28–31*). The spectrum of neural oscillations has been thought to emerge from competition between local oscillators since different oscillations can naturally emerge in neural networks with different cell-type compositions (*17*). Our findings suggest that individual neurons can control the frequencies of their network oscillations via a membrane-mixing phenomenon. The neural mixing capacity may exert a top-down modulation of oscillation-dependent cognitive functions.

Our data show that each brain region has a unique pattern of mixing oscillations modulated by inter-regional mixing, suggesting a mechanism coupling local and global oscillations. Yet, we did not test the direct link between frequency mixing at the cellular and network levels. Future studies using concurrent single-cell and network-level recording may be able to elucidate this link. The functional role of neural oscillations has been linked to the coordination of spiking activity between brain sites because we have observed task-induced synchronization, i.e., phase alignment, also known as functional connectivity (*27*). Our results imply that neurons could directly utilize these oscillations to perform advanced computational operations such as phase detection and de/multiplexing that, until now, have only been seen in modern telecommunication.

References and Notes

1. A. Goldsmith, Wireless communications. *Wirel. Commun.* 9780521837, 1–644 (2005).
2. V. V. Protopopov, Principles of optical heterodyning. *Springer Ser. Opt. Sci.* (2010), doi:10.1007/978-3-642-02338-5_1.
3. N. Grossman, D. Bono, N. Dedic, S. B. Kodandaramaiah, A. Rudenko, H.-J. Suk, A. M. Cassara, E. Neufeld, N. Kuster, L.-H. Tsai, A. Pascual-Leone, E. S. Boyden, Noninvasive Deep Brain Stimulation via Temporally Interfering Electric Fields. *Cell.* 169, 1029–1041 (2017).

4. F. H. Kasten, E. Negahbani, F. Fröhlich, C. S. Herrmann, Non-linear transfer characteristics of stimulation and recording hardware account for spurious low-frequency artifacts during amplitude modulated transcranial alternating current stimulation (AM-tACS). *Neuroimage* (2018), doi:10.1016/j.neuroimage.2018.05.068.

5. A. Poleg-Polsky, J. S. Diamond, NMDA Receptors Multiplicatively Scale Visual Signals and Enhance Directional Motion Discrimination in Retinal Ganglion Cells. *Neuron* (2016), doi:10.1016/j.neuron.2016.02.013.

6. M. Lavzin, S. Rapoport, A. Polsky, L. Garion, J. Schiller, Nonlinear dendritic processing determines angular tuning of barrel cortex neurons in vivo. *Nature* (2012), doi:10.1038/nature11451.

7. F. Gabbiani, H. G. Krapp, C. Koch, G. Laurent, Multiplicative computation in a visual neuron sensitive to looming. *Nature* (2002), doi:10.1038/nature01190.

8. L. N. Groschner, J. G. Malis, B. Zuidinga, A. Borst, A biophysical account of multiplication by a single neuron. *Nature* (2022), doi:10.1038/s41586-022-04428-3.

9. E. Mirzakhalili, B. Barra, M. Capogrosso, S. F. Lempka, Biophysics of Temporal Interference Stimulation. *Cell Syst.* (2020), doi:10.1016/j.cels.2020.10.004.

10. D. Haufler, D. Paré, Detection of Multiway Gamma Coordination Reveals How Frequency Mixing Shapes Neural Dynamics. *Neuron* (2019), doi:10.1016/j.neuron.2018.12.028.

11. H. O. Lancaster, "Chi-Square Distribution" in *Encyclopedia of Statistical Sciences* (2004).

12. P. K. Rubenstein, K. P. Chwialkowski, A. Gretton, "A kernel test for three-variable interactions with random processes" in *32nd Conference on Uncertainty in Artificial Intelligence 2016, UAI 2016* (2016).

13. D. Sejdinovic, A. Gretton, W. Bergsma, "A kernel test for three-variable interactions" in *Advances in Neural Information Processing Systems* (2013).

14. S. B. Kodandaramaiah, G. T. Franzesi, B. Y. Chow, E. S. Boyden, C. R. Forest, Automated whole-cell patch-clamp electrophysiology of neurons in vivo. *Nat. Methods*. 9, 585–7 (2012).

15. J. O'Keefe, M. L. Recce, Phase relationship between hippocampal place units and the EEG theta rhythm. *Hippocampus* (1993), doi:10.1002/hipo.450030307.

16. A. Bollimunta, Y. Chen, C. E. Schroeder, M. Ding, Neuronal mechanisms of cortical alpha oscillations in awake-behaving macaques. *J. Neurosci.* (2008), doi:10.1523/JNEUROSCI.2699-08.2008.

17. G. Buzsáki, A. Draguhn, Neuronal olscillations in cortical networks. *Science (80-.).* (2004), , doi:10.1126/science.1099745.

18. K. F. Ahrens, H. Levine, H. Suhl, D. Kleinfeld, Spectral mixing of rhythmic neuronal signals in sensory cortex. *Proc. Natl. Acad. Sci. U. S. A.* (2002), doi:10.1073/pnas.222547199.

19. G. Buzsáki, N. Logothetis, W. Singer, Scaling brain size, keeping timing: Evolutionary preservation of brain rhythms. *Neuron* (2013), , doi:10.1016/j.neuron.2013.10.002.

20. H. Berger, Über das Elektrenkephalogramm des Menschen. *Arch. Psychiatr. Nervenkr.*

(1929), doi:10.1007/BF01797193.

21. P. Fries, J. H. Reynolds, A. E. Rorie, R. Desimone, Modulation of oscillatory neuronal synchronization by selective visual attention. *Science (80-.).* (2001), doi:10.1126/science.1055465.

22. M. Carrasco, Visual attention: The past 25 years. *Vision Res.* (2011), , doi:10.1016/j.visres.2011.04.012.

23. A. Hampshire, R. R. Highfield, B. L. Parkin, A. M. Owen, Fractionating Human Intelligence. *Neuron* (2012), doi:10.1016/j.neuron.2012.06.022.

24. D. Kleinfeld, S. B. Mehta, "Spectral mixing in nervous systems: Experimental evidence and biologically plausible circuits" in *Progress of Theoretical Physics Supplement* (2006).

25. B. Doiron, A. Litwin-Kumar, R. Rosenbaum, G. K. Ocker, K. JosiC, The mechanics of state-dependent neural correlations. *Nat. Neurosci.* (2016), , doi:10.1038/nn.4242.

26. J. Keil, D. Senkowski, Neural Oscillations Orchestrate Multisensory Processing. *Neuroscientist* (2018), , doi:10.1177/1073858418755352.

27. L. M. Ward, Synchronous neural oscillations and cognitive processes. *Trends Cogn. Sci.* (2003), , doi:10.1016/j.tics.2003.10.012.

28. P. J. Uhlhaas, W. Singer, Neural Synchrony in Brain Disorders: Relevance for Cognitive Dysfunctions and Pathophysiology. *Neuron*. 52, 155–168 (2006).

29. V. Nimmrich, A. Draguhn, N. Axmacher, Neuronal Network Oscillations in Neurodegenerative Diseases. *NeuroMolecular Med.* (2015), doi:10.1007/s12017-015-8355-9.

30. E. Başar, Brain oscillations in neuropsychiatric disease. *Dialogues Clin. Neurosci.* (2013), doi:10.31887/dcns.2013.15.3/ebasar.

31. S. Vanneste, J. J. Song, D. De Ridder, Thalamocortical dysrhythmia detected by machine learning. *Nat. Commun.* (2018), doi:10.1038/s41467-018-02820-0.

Acknowledgments: We thank Lok Fan for improving computational efficiency, Yuval Gal Shohet for discussions on JHOI measure, Dr Ho-Jun Suk for assisting with *in vivo* patch-clamp experiments, and Dr Carola Radulescu and Dr Sam Barnes for help in setting up the *ex vivo* patch-clamp experimental rig.

Funding:

Deutsche Forschungsgemeinschaft, DFG, German Research Foundation, Project-ID 424778381-TRR 295 (RP)

EPSRC award EP/N014529/1 supporting the EPSRC Centre for Mathematics of Precision Healthcare at Imperial College London (RP, FL, MB)

UK Dementia Research Institute—an initiative funded by the Medical Research Council (NG)

Engineering and Physical Sciences Research Council, UK, EP/W004844/1 (NG)

National Institute for Health and Care Research, Imperial Biomedical Research Centre (NG)

Author contributions:

Conceptualization: NG, CL, RP

Methodology: CL, RP, FL

Investigation: CL, RP, EJM

Visualization: CL, RP, ER

Supervision: NG, MB, ESB, DJS

Writing: NG, CL, RP, ER, EJM

Competing interests: NG. and ESB are inventors of a patent on neuromodulation using temporal interference (TI) of kHz electric fields, assigned to MIT. NG and ESB are co-founders of TI Solutions AG, a company committed to producing hardware and software solutions to support TI research.

Data and materials availability: All data, code, and materials used in the analysis are available from the corresponding author upon request.

(We will also deposit all the data and code on a public repository once the manuscript is in its final form, i.e., upon completion of the review and before publication)

Supplementary Materials

Materials and Methods

Figs. S1 to S7

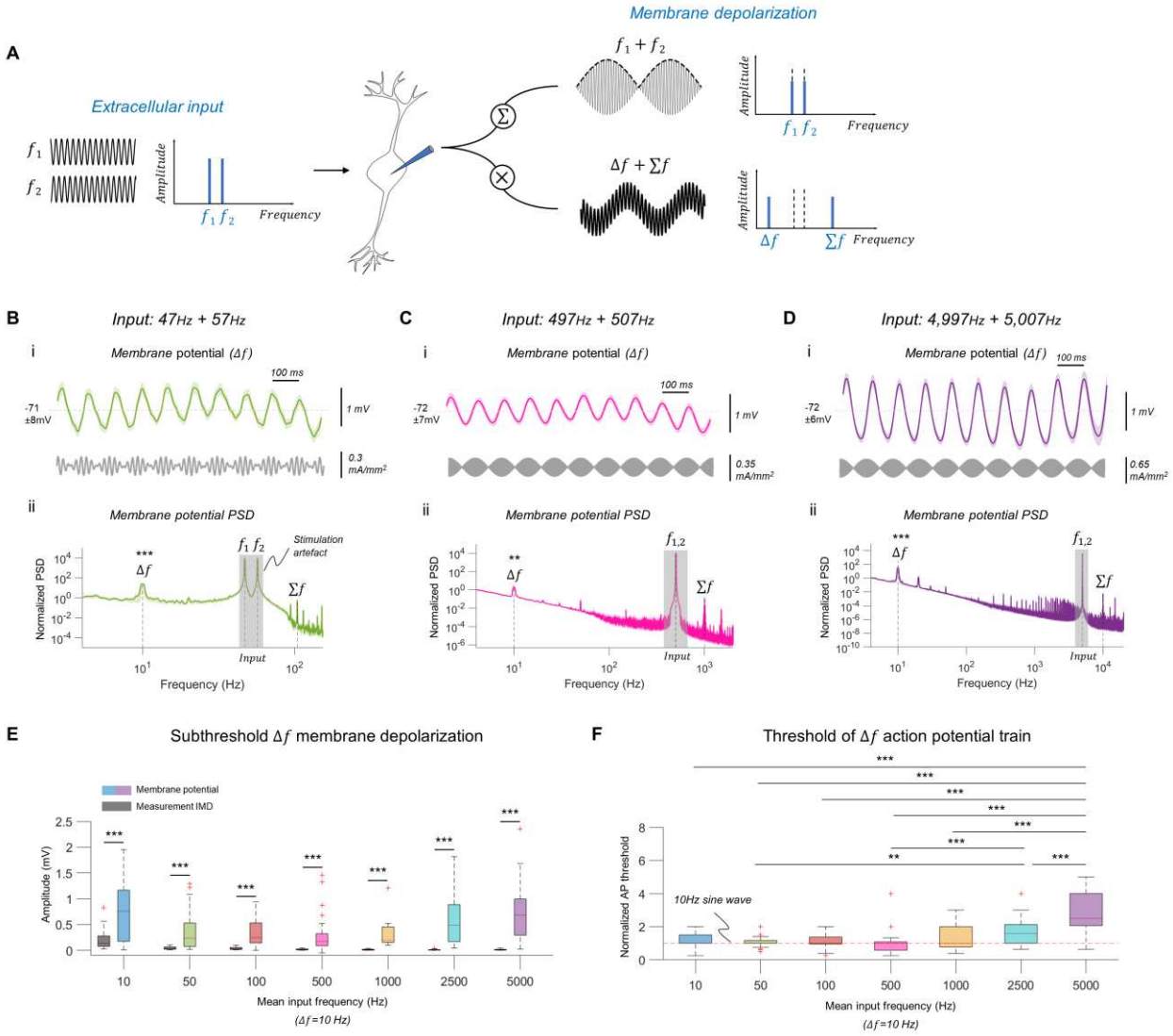

Fig. 1. Mixing of exogenous membrane potentials in individual neurons *ex vivo*. (**A**) Neural mixing concept showing the subthreshold membrane transfer function of multi-frequency input with a conventional linear superposition ('∑'), and the proposed nonlinear mixing via multiplication ('X'). (**B**) (i) Top: Neural membrane potential during sinusoidal electrical stimulation with frequencies f_1=47Hz + f_2=57Hz (shown are mean ±SEM). Resting membrane potential mean ±SD is displayed. Raw membrane traces were filtered to remove stimulation artefact; n=26 cells. Bottom: Applied stimulation current waveform. (ii) Corresponding membrane potential's power spectral density (PSD), mean ±SEM. Raw membrane traces were first filtered to remove offset. PSD values were normalised to endogenous PSD activity at 4Hz; n=26 cells. PSD at f_1 and f_2 is dominated by stimulation artefact. ***, p<0.0005, significant PSD peak, one tailed Wilcoxon signed rank test for zero median. (**C**) As in (B) but during stimulation with f_1=497Hz + f_2=597Hz; n=31 cells. **, p<0.005, one tailed Wilcoxon signed rank test for zero median. (**D**) As in (B) but during stimulation with f_1=4997Hz + f_2=5007Hz; n=33 cells. (**E**) Box plot showing root mean square (RMS) amplitude of the induced neural oscillation at Δf ('Membrane potential') vs. the measurements' IMD at Δf ('Measurement IMD') across the range of stimulation frequencies. Traces were first filtered at Δf. RMS values

were baseline-subtracted. n (IMD/Membrane potential) = 27/31 (10Hz); 21/27 (50Hz); 27/29 (100Hz); 26/30 (500Hz); 16/22 (1,000Hz); 29/29 (2,500Hz); 29/32 (5,000Hz) recordings/cells. ***, $p < 0.0005$, Wilcoxon rank sum test. Current densities: 0.38±0.30(10Hz); 0.29±0.22(50Hz); 0.36±0.27(100Hz); 0.34±0.27(500Hz); 0.32±0.28 (1,000Hz); 0.45±0.35 (2,500Hz); 0.66±0.36 (5,000Hz) mA/mm^2. (**F**) Normalised current threshold for action potential (AP) train at Δf across the range of stimulation frequencies. Thresholds were normalised to threshold of a stimulation with 10Hz sine wave (horizontal red dashed line). *, comparisons survived Bonferroni correction (p-value=0.0021); **, p<0.005; ***, p<0.0005; repeated-measures ANOVA, post-hoc paired t-test. Boxplots: central mark, median; box edges, 25th and 75th percentiles; whiskers, extend up to 1.5x interquartile range box edges; '+', datapoints outside this range.

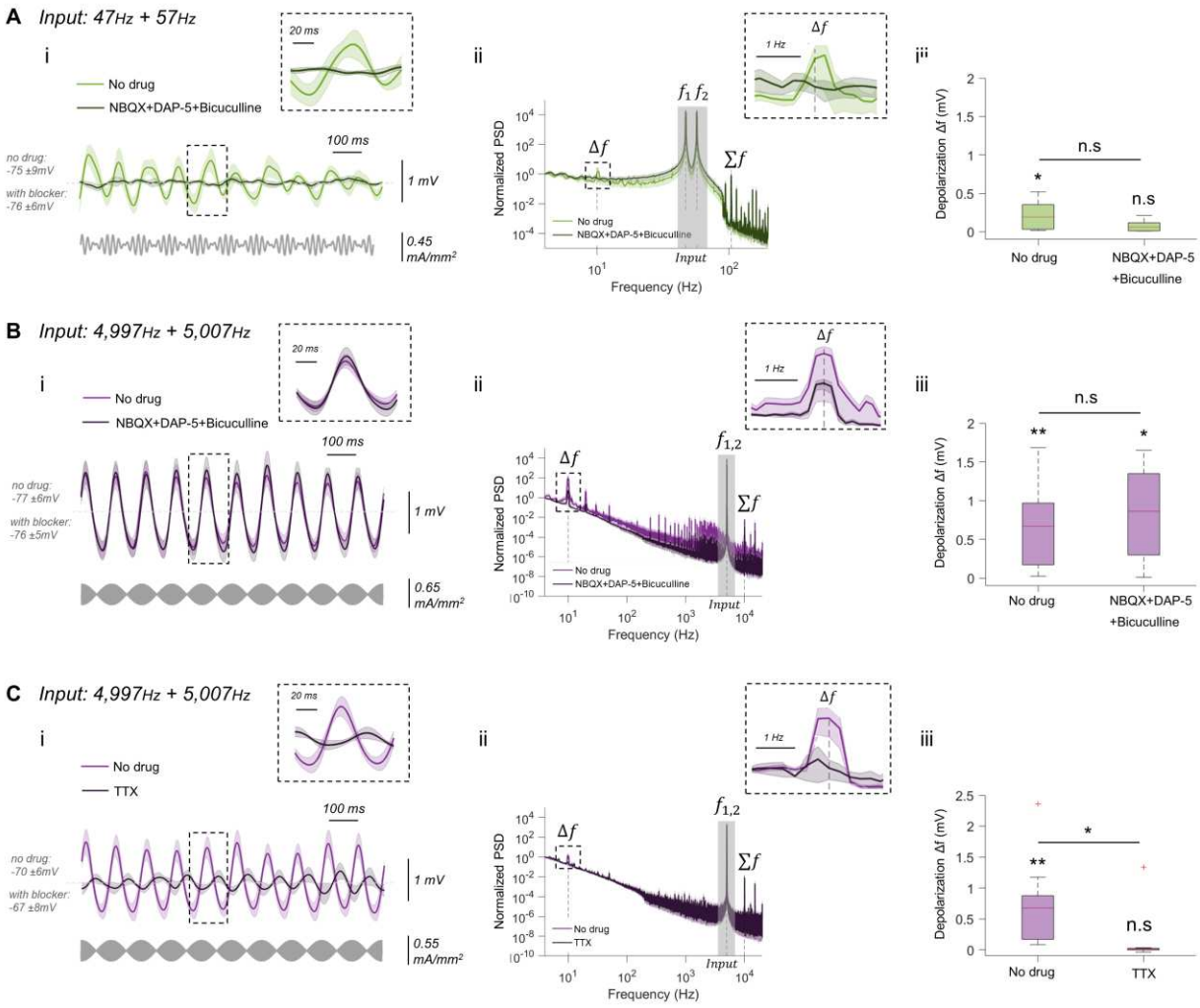

Fig. 2. Origin of neuronal mixing characterized via pharmacological manipulation *ex vivo*. (**A**) (**i**) Membrane potential during stimulation with sinusoidal electrical stimulation with f_1=47Hz + f_2=57Hz, before (colour) and during (grey) pharmacological blockade of synaptic NMDA, AMPA, and GABA-A ion channel currents (shown are mean ± SEM). Raw membrane traces were filtered to remove stimulation artefact. Resting membrane potential mean ± SD is displayed. n=8 cells. Bottom: Applied stimulation current waveform. Zoom view of boxed region at the difference frequency (Δf) is included. (**ii**) Membrane potential PSD during the

stimulation in (A). Raw membrane traces were first filtered to remove offset. PSD values were normalised as in (1Bii). n = 8 cells. Zoom view of boxed region is included. (**iii**) Box plots of RMS amplitude of the induced neural oscillation at Δf during the stimulation in (i) without drug and with drug. RMS values were baseline-subtracted. * above each box indicates significant oscillation at Δf relative to measurement's IMD at Δf. *, $p < 0.05$, two sample t-test. * between boxes indicates difference between drug conditions, paired t-test. n.s, non-significant. n(IMD/membrane potential)=8/8 recordings/cells. (**B**) As in (A) but during stimulation with f_1 = 4997Hz + f_2 = 5007Hz. n=9 cells. n (IMD/membrane potential) = 8/9 recordings/cells. *, $p < 0.05$; **, $p < 0.005$. (**C**) As in (B) but before (colour) and during (grey) pharmacological blockade of TTX-sensitive conductance. (IMD/ membrane potential) = 11/11 recordings/cells. Boxplots: central mark, median; box edges, 25th and 75th percentiles; whiskers, 1.5x interquartile range; '+', datapoints outside this range.

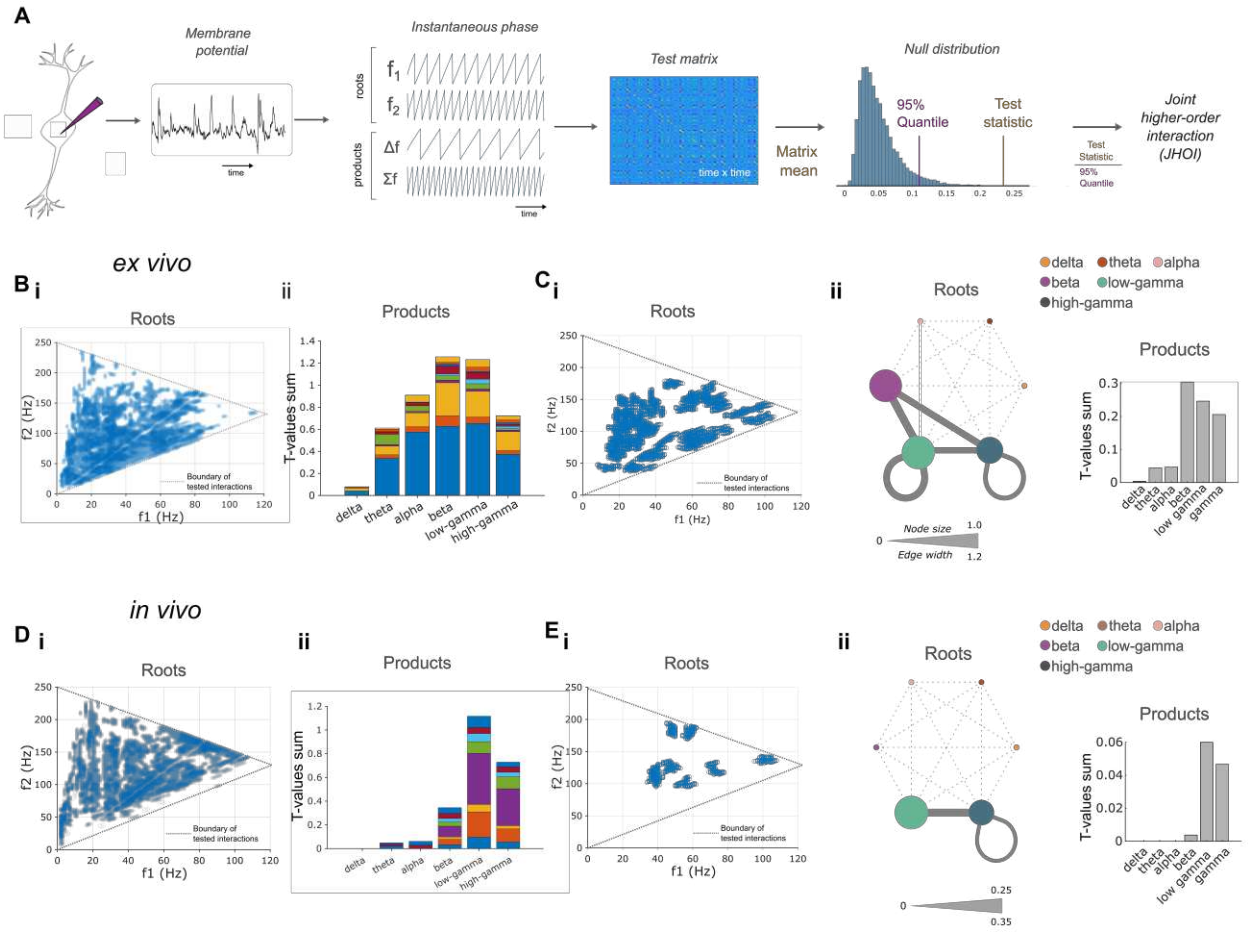

Fig. 3. Endogenous membrane potential mixing in individual neurons *ex vivo* and *in vivo*. (**A**) Workflow to assess endogenous frequency mixing in cell membrane potential. For a given trace of endogenous membrane potential, the instantaneous phases of four frequency mixing components (roots: $f_1, f_2 > f_1$, products: $\Delta f = f_2 - f_1, \sum f = f_1 + f_2$) are extracted. Each subset of three phases (triplet) are used to construct a test matrix, which, when compared to a null distribution, defines the joint higher-order interaction (JHOI) strength heuristic. (**B**-**C**) *Ex vivo* recordings. (**B**) Frequency quadruplets with significant mixing, shown are (i) distribution of mixing root frequencies overlaid and (ii) distribution of mixing product frequencies coloured by

individual cell, stacked by frequency band. n=20 cells. (**C**) Frequency quadruplets with significant mixing consistent across the cells (i.e., group-level), showing (i) distribution of root frequencies overlaid, (ii) root frequencies stratified by frequency bands (network plot†), and distribution of frequency mixing products (bar chart). n=20 cells. (**D**-**E**) *In vivo* recordings. (**D**) As in (B) but *in vivo*. (**E**) As in (C) but *in vivo*. †Network plots: node size proportional to normalised sum of t-values of significant quadruplets within band (t-test vs. surrogate), edge width as in node size for roots shared between bands.

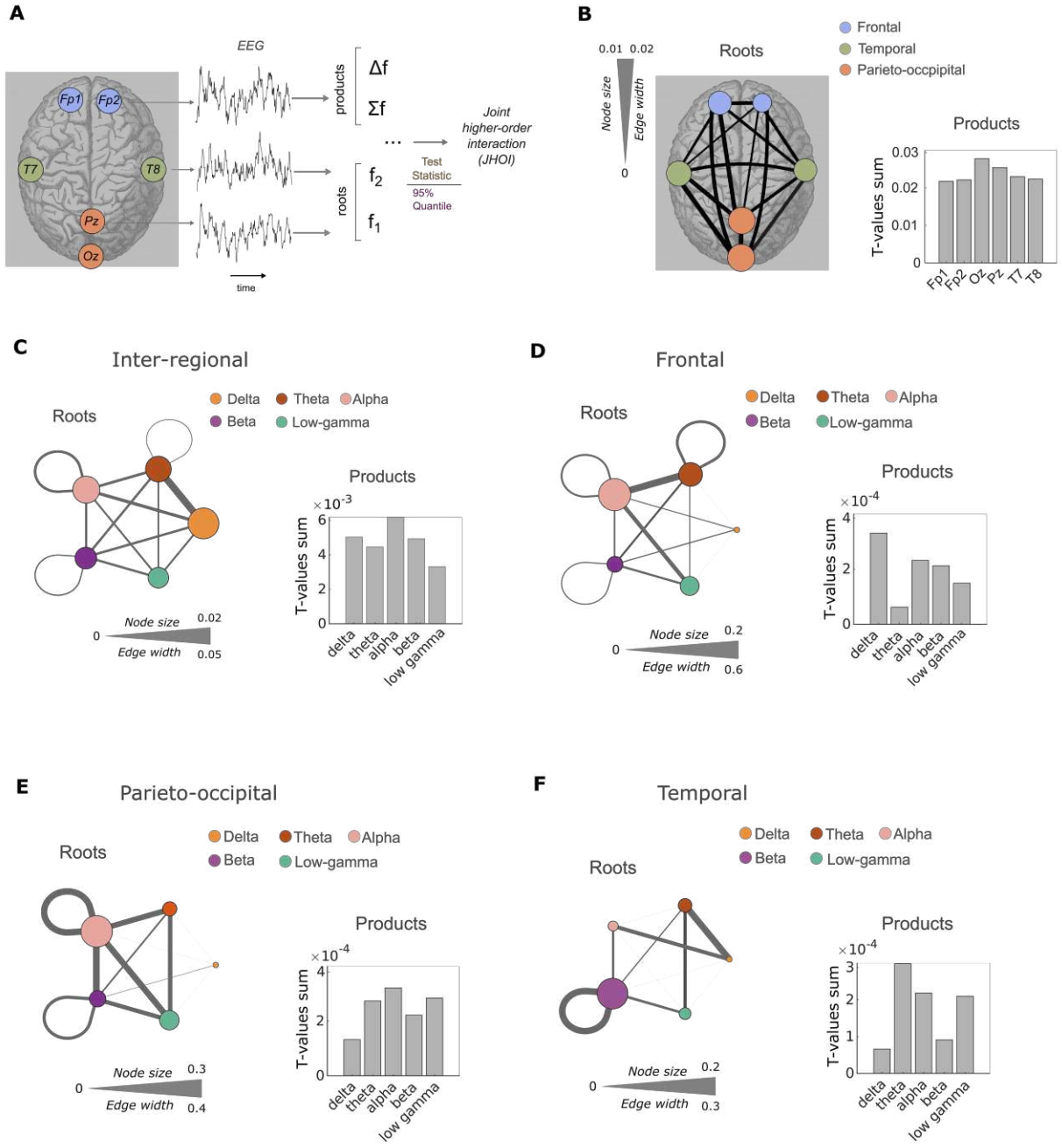

Fig. 4. Mixing of endogenous neural network oscillations in the human brain EEG. (**A**) Illustration of workflow for assessing endogenous frequency mixing in the human brain EEG. Similar to (3A) but with instantaneous phases of the four frequency mixing components

extracted from one or multiple cortical locations (in this example, roots: Pz and T8; products: Fp2). (**B-C**) Mixing of neural network oscillations between cortical sites. (**B**) Spatial topology of frequency mixing (significant at group-level against surrogate) for roots† (network plot) and products (bar chart). (**C**) Bands topology of frequency mixing (significant at group-level against surrogate) for roots† (network plot) and products (bar chart). (**D-F**) Mixing of neural network oscillations within cortical sites. (**D**) Bands topology of frequency mixing (significant at group-level against surrogate) in the frontal brain region for roots† and products (network plot). (**E**) As in (D) but in the parieto-occipital brain region. (**F**) As in (D), but in the temporal brain region. †Network plots: node size proportional to normalised sum of t-values of significant quadruplets within band/channel (t-test against surrogate), edge width same as node size but for roots shared between bands/channels. Boxplots: central line, median; circle, mean; whiskers, interquartile range; grey dots, outliers.

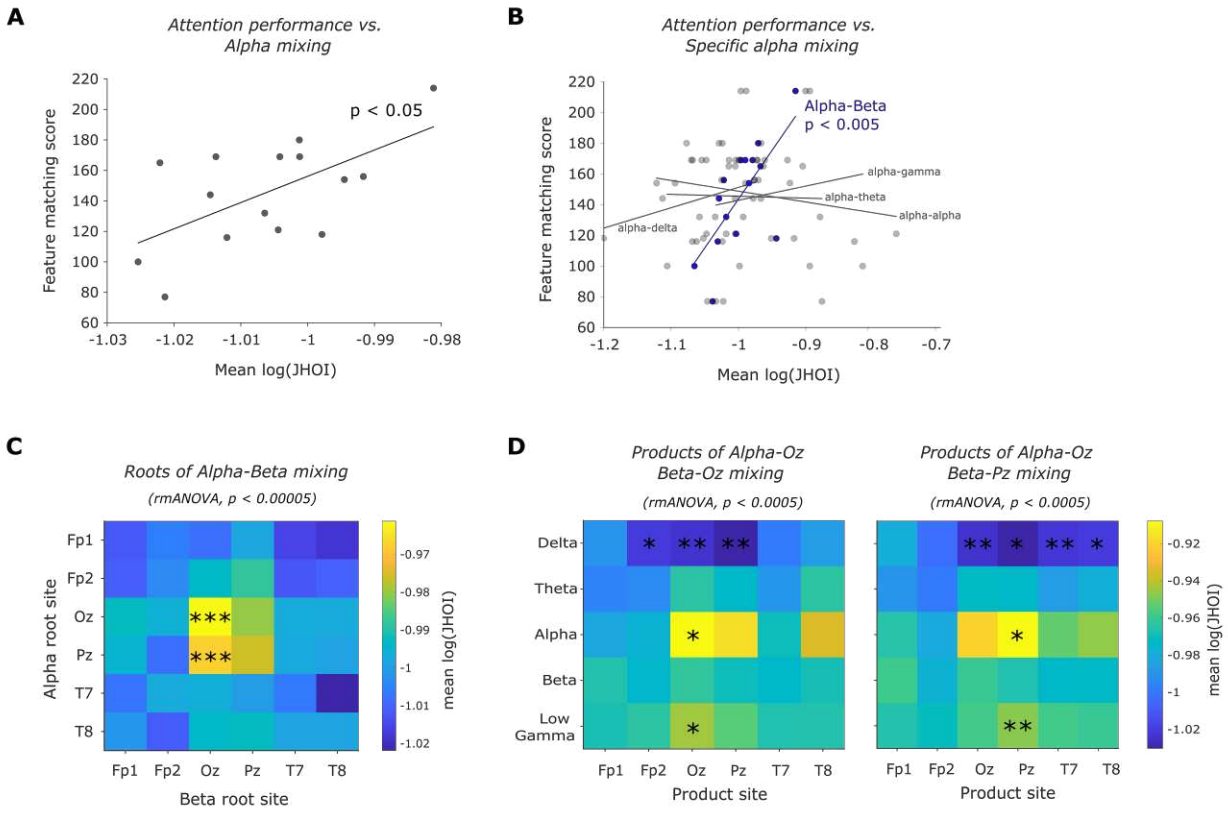

Fig. 5. Human network oscillation mixing correlates with visual attention control. (**A**) Participants' feature matching score vs strength of all alpha oscillation mixings (log JHOI averaged across all inter-site and local mixings), R^2= 0.363, p=0.017, linear regression. (**B**) Participants' feature matching score vs strength of alpha oscillation mixing with specific bands, showing significance at alpha-beta mixing, R^2= 0.497, p=0.003, linear regression, Bonferroni corrected for multiple comparisons. (**C**) Topology of attentional correlated alpha-beta mixing roots, showing strongest mixing within Oz and between Oz alpha and Pz beta. ***, p<0.001, post-hoc paired t-test comparisons. (**D**) Topology of alpha-beta mixing products originated in Oz alpha-Oz beta (left panel) and Oz alpha-Pz beta (right panel), showing strongest products in posterior alpha and gamma bands and weakest products at delta band. *, p<0.05, **; p<0.01; post-hoc paired t-test comparisons. rmANOVA, repeated measures ANOVA.